



OPEN

Interpretable real-time monitoring of short-term rockbursts in underground spaces based on microseismic activities

Mohammad Hossein Kadkhodaei[✉] & Ebrahim Ghasemi

In this study, two novel hybrid intelligent models were developed to evaluate the short-term rockburst using the random forest (RF) method and two meta-heuristic algorithms, whale optimization algorithm (WOA) and coati optimization algorithm (COA), for hyperparameter tuning. Real-time predictive models of this phenomenon were created using a database comprising 93 case histories, taking into account various microseismic parameters. The results indicated that the WOA achieved the highest overall performance in hyperparameter tuning for the RF model, outperforming the COA. RF-WOA model accurately predicted the occurrence of this phenomenon with an accuracy of 0.944. Additionally, for this model, precision, recall and F1-score were obtained as 0.950, 0.944 and 0.943, respectively, indicating that the proposed model is robust in predicting damage severity of rockburst in deep underground projects. Subsequently, the Shapley additive explanations (SHAP) method was employed to interpret and explain the prediction process and assess the influence of input features based on RF-WOA model. The results showed that three parameters including cumulative seismic energy, cumulative microseismic events, and cumulative apparent volume have the greatest impact on the occurrence of rockburst events. This study provides an interpretable and transparent resource for accurately predicting rockburst events in real time. It can facilitate estimating project costs, selecting a suitable support system, and identifying essential ways to limit the danger of rockburst.

Keywords Short-term rockburst, Microseismic monitoring, Random forest, Whale optimization algorithm, Coati optimization algorithm

The phenomenon of rockburst (RB) refers to a dynamic failure (seismic event) that occurs due to the violent and sudden release of elastic energy accumulated within coal or rock formations. This phenomenon can result in significant consequences, including the failure of underground working spaces, potential casualties, deformation of supporting systems, damage to machinery, and delays in construction activities^{1–4}. Based on these destructive effects, attention needs to be given to predicting of this phenomenon in underground excavation projects. There are two types of RB prediction: long-term and short-term^{5–8}. The long-term prediction of RB is typically conducted during the early stages of excavation and project design, and it serves as a guide for the subsequent excavation phases. Such predictions typically rely on intrinsic rock mechanics parameters (including stiffness, strength, energy storage capacity, and brittleness) to assess the occurrence of this phenomenon at a specific site. On the other hand, short-term prediction is primarily used during the life of the project to quickly detect the occurrence of RB events. This enhances the coordination of industrial activities and reduces the risk of severe accidents. Generally, short-term RB prediction involves assessing the risk of RB occurrences in the near future based on in situ techniques. Among these techniques, microseismic (MS) monitoring is one of the most widely used methods for RB event monitoring due to real-time monitoring, wide detection range, big data scale, and no harm to production^{8,9}. In this technique, using sensors laid out spatially with different azimuths, MS waves released during rock fracture can be captured. By analyzing the MS waves, some precursory features of RB events are discovered that could be used to predict the risk of this phenomenon^{10–12}.

The mechanism of RB occurrence is complex and influenced by a combination of factors. Because of this complexity, RB prediction without the aid of computer models is challenging¹³. Recently, machine learning (ML) methods have been employed to predict RB owing to their capacity to tackle complex and nonlinear

Department of Mining Engineering, Isfahan University of Technology, Isfahan 8415683111, Iran. [✉]email: mh.kadkhodaei@mi.iut.ac.ir

issues⁷. These methods mainly focus on the long-term prediction of this phenomenon using unsupervised learning, supervised learning, and comparative decision strategies^{14–43}, whereas only a few studies have been conducted on short-term prediction using ML methods^{6,44–48}. Based on literature survey, application of ML methods has proven to be effective in real time prediction of RB intensity based on MS monitoring data. Despite their reliable and precise outputs, most algorithms are not readily applicable in practice owing to their non-interpretable “black box” nature. Also, development of ML models requires fine-tuning hyperparameters, which can drastically affect the performance of a model⁴⁹. Fine-tuning hyperparameters is a computational challenge due to the large size of search space. There are a variety of methods for finding the optimal Hyperparameters. In most previously developed models, adjusting of hyperparameters was done manually, which requires a lot of time and trial and error⁵⁰. Recently, to solve this problem, the optimization methods are used as a practical way from the perspective of time and performance balance.

To address the mentioned limitations of traditional ML models, this study proposes two novel hybrid models for short-term prediction of RB intensity. Two models are developed in the Python environment using the random forest (RF) method, with whale optimization algorithm (WOA) and coati optimization algorithm (COA) applied to adjust the hyperparameters. The RF technique was chosen due to its outstanding capability in addressing complex and nonlinear problems such as RB prediction. Additionally, the Shapley additive explanations (SHAP) method is applied to explain the prediction process and assess the influence of input features.

Database description

The study utilized a database collected from MS monitoring events of the Jinping-II hydropower project in China to develop the proposed models⁵¹. The Jinping-II hydropower project is located at the Jinping bend on the Yalong River and the main characteristics of this case study are presented in Table 1. During construction process of this project, RB events occurred frequently and caused significant problems in terms of safety. According to site observation and survey, all three types of RB (including strain burst, pillar burst and slip-fault burst) occurred, while strain bursts were the most common⁵². In strain bursts, the location of the seismic event is the same as where damage occurs, providing the opportunity to predict the RB using MS monitoring data⁶. MS monitoring system was built based on the Integrated Seismic System (ISS), including a server, smart sensors, geophysical seismometer (GS), intelligent uninterruptible power system (UPS), optional communication element (I-Splitter, moxa, fiber, DSL, and TP-Link), junction box, cables, etc. A 54-channel MS monitoring system was used and the GS had a wide sampling rate (3–48,000 Hz)^{10,52}. The MS sensors had a natural frequency of 14 Hz and an approximate usable frequency range that varied from 7 to 2000 Hz. Two groups of MS sensors were set up just behind the working face. These were moved with the working face every 30–40 m (i.e. manually removed, moved, and set up again). A sectional velocity model was used for MS events location. Details of the MS data acquisition system has been discussed in Feng et al.¹⁰.

The database includes 93 RB case histories. Based on this database, the input parameters for developing hybrid intelligent models are cumulative seismic energy (CE), cumulative microseismic events (ME), cumulative apparent volume (CV), event rate (ER), apparent volume rate (AVR), seismic energy rate (LER) and the output is RB severity related to each case⁵¹. Based on literature survey, these six input parameters are most commonly used MS features to predict the severity of RB in real-time. ME denotes the measure of microfracture density, while CV and CE denote the extent of damage and the fracture strength to the rock mass, respectively. These three parameters are fundamental indicators representing the attributes of microfractures during the development of RB events¹⁰. To integrate temporal aspects into the process, three parameters related to time (ER, AVR, and LER) are considered. ER denotes the rate of MS activity occurrence, the process of rock mass failure, and the average response pattern over time. LER indicates the energy emitted by the rock mass through MS radiation during a specific time period, while AVR refers to the volume of rock within the deformation region experiencing inelastic behavior over the same time frame⁶. To optimize execution, the values of LER, AVR, CV, and CE are chosen on a logarithmic scale. The primary objective of the logarithmic function is to address the skewness towards larger numbers in the RB database. Figure 1 shows the histograms, cumulative distributions, and basic statistical description of input parameters. The RB severity (output parameter) is classified into four classes (including none, light, moderate, and severe) based on the classification by Chen et al.⁵², the distribution of which is shown in Fig. 2.

Physical characteristics	The project includes seven parallel tunnels (four headrace tunnels, two assistant tunnels, and one drainage tunnel)
	The average length of each tunnel is 16.67 km
	The maximum depth of the tunnels is 2525 m
	The maximum, intermediate and minimum principal stresses are 63 MPa, 34 MPa and 26 MPa, respectively
Lithological characteristics	The main lithology is marble
	The saturated uniaxial compressive strength ranges from 30 to 114 MPa
	The elastic modulus ranges from 25 to 40 GPa
	The tensile strength ranges from 3 to 6 MPa
	The surrounding rock masses are hard and intact

Table 1. Characteristics of Jinping-II hydropower project^{45,53,54}.

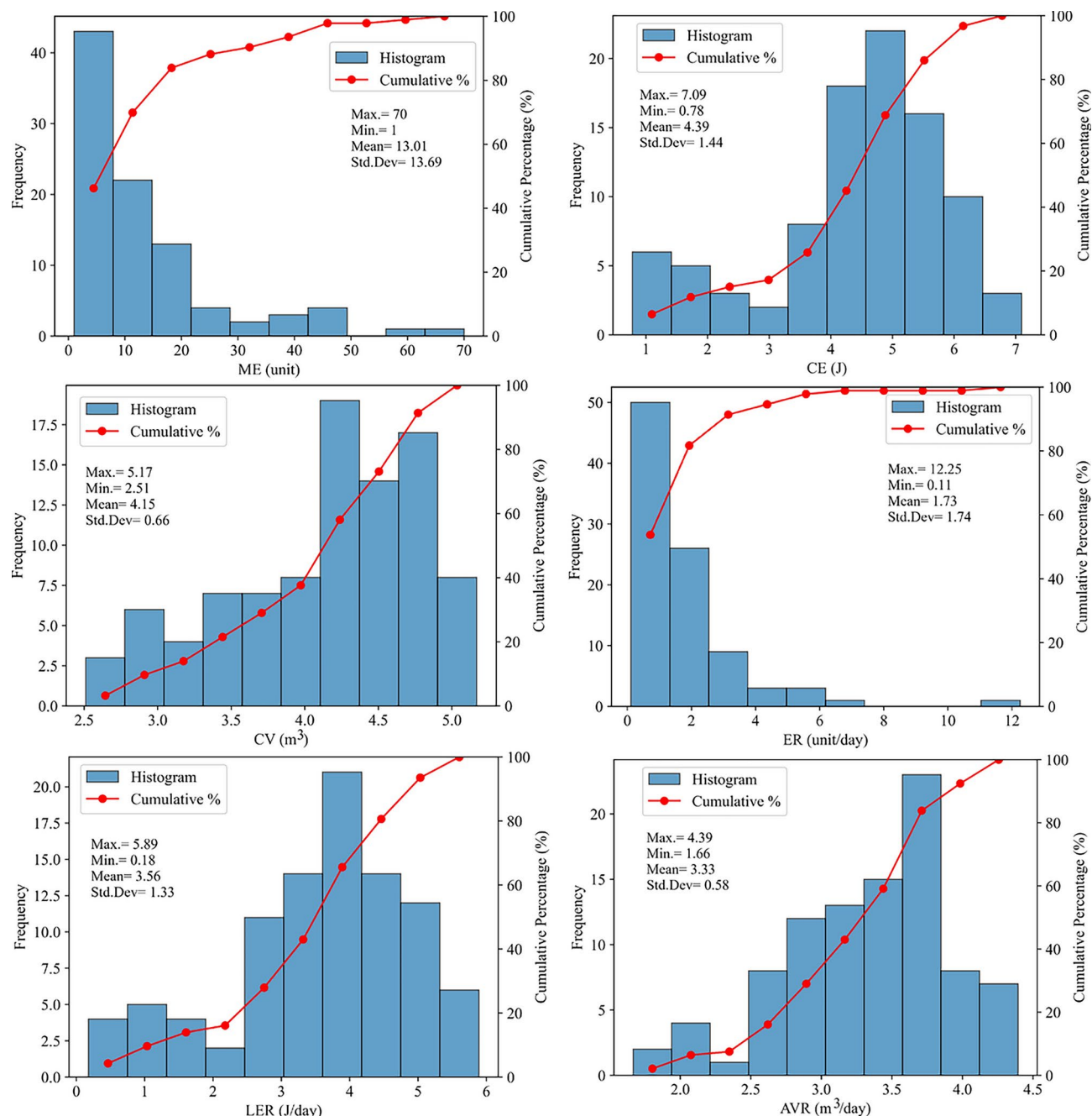
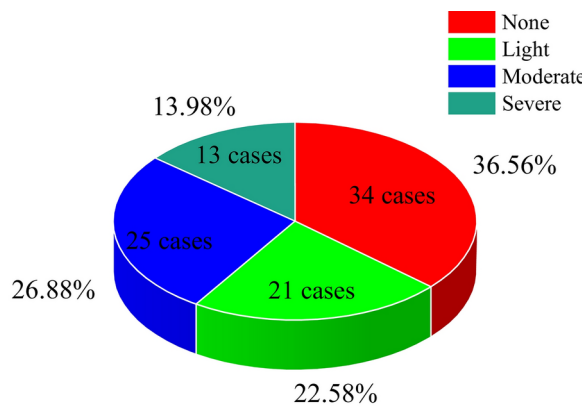


Fig. 1. The histogram, cumulative distribution, and basic statistical description of input parameters.

Development of models

RF is an integrated learning method based on decision trees, which enhances the generalizability and accuracy of the model by constructing multiple decision trees and averaging their predictions, or selecting the final prediction through majority vote⁵⁵. The RF algorithm is an extension of the bagging integration method. It utilizes bagging and feature randomness to generate a set of uncorrelated decision trees, consequently diminishing correlations between them and enhancing model diversity⁵⁶. This approach mitigates the risk of overfitting, enhances model robustness, facilitates feature importance assessment, and enables parallelized training, thereby significantly reducing training time. In the development of real-time models, the optimal selection of hyperparameters affects the performance and accuracy of the models. In this study, the WOA meta-heuristic algorithm has been utilized to optimally adjust hyperparameters. Mirjalili et al.⁵⁷ introduced WOA, a novel meta-heuristic optimization algorithm, in 2016. This algorithm enhances performance by mimicking the hunting behavior of humpback whales. The specific implementation method entails replicating the bubble-net feeding technique of humpback whales through a spiral pattern⁵⁸. The bubble-net feeding technique comprises three sequential steps: encircling the prey, creating a spiral bubble-net to trap the prey, and then locating the next target⁵⁹. Since the method and



None: No obvious surface failure; nearly no cracking sound; no damaged support system

Light: Light spalling or slabbing; 10–30 cm ejected rock fragment size; light cracking sound; failure depth less than 0.5 m; no damaged support system

Moderate: Severe spalling and slabbing; 30–80 cm ejected rock fragment size with; cracking sound like a detonator blasting; 0.5–1.0 m failure depth; damaged shotcrete lining between rock bolts

Severe: Large volume of rock mass ejected; 80–150 cm ejected rock fragment size; fresh fracture planes in the failure zone; lasting sound like an explosive with an impact wave; 1.0–3.0 m failure depth; support system destroyed

Fig. 2. Distribution of the RB severity classes.

mathematical aspects of WOA have already been extensively documented in numerous literature sources^{59–62}, this study does not provide an explanation of them. The RF algorithm was utilized in the Python environment in this section, and its performance was improved by optimizing it with the WOA. RF serves as the framework for developing models, utilizing the WOA to determine the best hyperparameters. To develop the models, the train-test (hold out cross validation) method was used. The database has been randomly partitioned into two segments: training and testing, in an 8:2 ratio. Initially, the model is trained on 80% of the data and subsequently validated using the remaining 20%. It is important to note that the test database is independent of the training database and plays no role in the model's development. Figure 3 shows the algorithm of RF hybrid models. Table 2 displays the optimal arrangement of RF-WOA hyperparameters.

Another optimization algorithm utilized in this study to adjust the hyperparameters of the RF algorithm is the COA. The COA is a novel metaheuristic algorithm introduced in 2023 by Dehghani et al.⁶³, inspired by the natural actions of coatis. It imitates two specific behaviors of coatis: hunting iguanas and evading predators. The implementation process of this algorithm includes three steps: 1) initialization process, 2) exploration phase, and 3) exploitation phase, the details of which have been elucidated by various researchers^{63,64}. Similar to the previous one, this algorithm is first developed in the Python environment using the training database and then evaluated on the test database. Table 3 displays the optimal arrangement of RF-COA hyperparameters.

Performance evaluation and comparison of models

The RF-WOA and RF-COA hybrid models are evaluated using the testing datasets. The performance of the models is thoroughly assessed in this section using precision, accuracy, F1-score, and recall measures⁶⁵. These values can be determined through the confusion matrices of each model (Fig. 4). Figures 5 and 6 show the confusion matrices of models RF-WOA and RF-COA (for both train and test datasets), respectively. The evaluation results of the created models, using assessment metrics, are displayed in Table 4. Based on the obtained results, the WOA optimizer shows superior performance in the RF model for evaluating the occurrence of RB compared to the COA optimizer.

To thoroughly assess the established models, they were compared with the recently created models in the literature for prediction of short-term RB potential (Table 5). This comparison, as part of the performance evaluation of the models, showed that the proposed RF-WOA model can accurately predict the RB severity with outstanding accuracy. This model overcomes the limitations of previous ML models applying WOA optimization algorithm for hyperparameters tuning of RF model and SHAP method to assess the influence of input features on RB severity (which is described in the next section). On the other hand, this model not only exhibits high prediction performance but also promotes transparency in the prediction process. Therefore, project managers can use this model to predict this phenomenon and implement the necessary control measures to increase safety and productivity.

Finally, to prove the applicability and practicability, RF-WOA model (as the best developed model) was utilized to predict 19 new RB cases, which were not included in the original 93 cases. These new validation cases were collected from the MS monitoring technique from the Jinping-II hydropower project in China, the Ashale Copper Mine in China, the Neelum-Jhelum Hydroelectric Tunnel in Pakistan and the Qinling Water Conveyance Tunnel in China^{72,73}. Table 6 presents the MS monitoring parameters with real and predicted RB severity for each case. As shown in Table 6, the prediction results of RF-WOA model are coincided with real RB

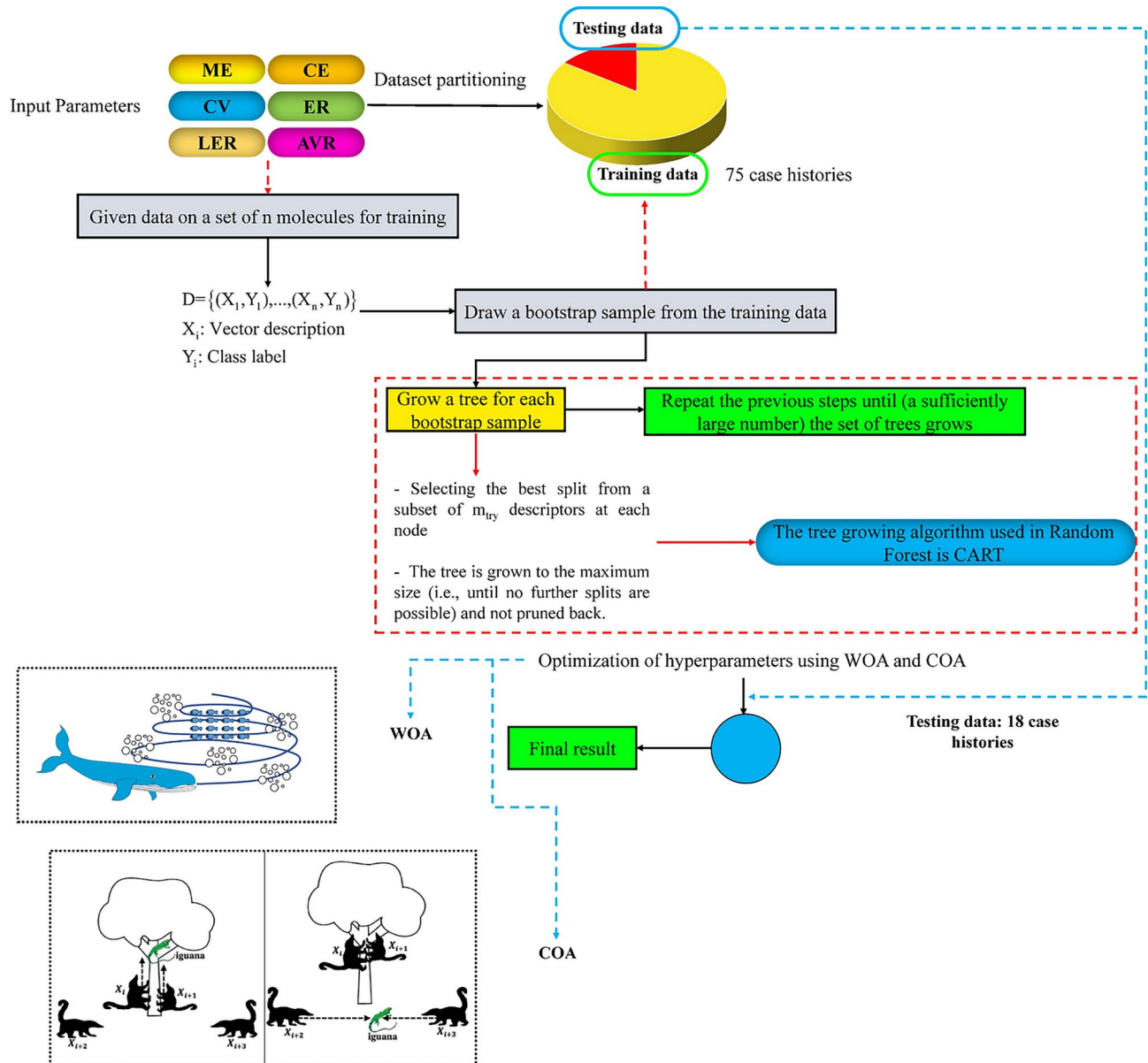
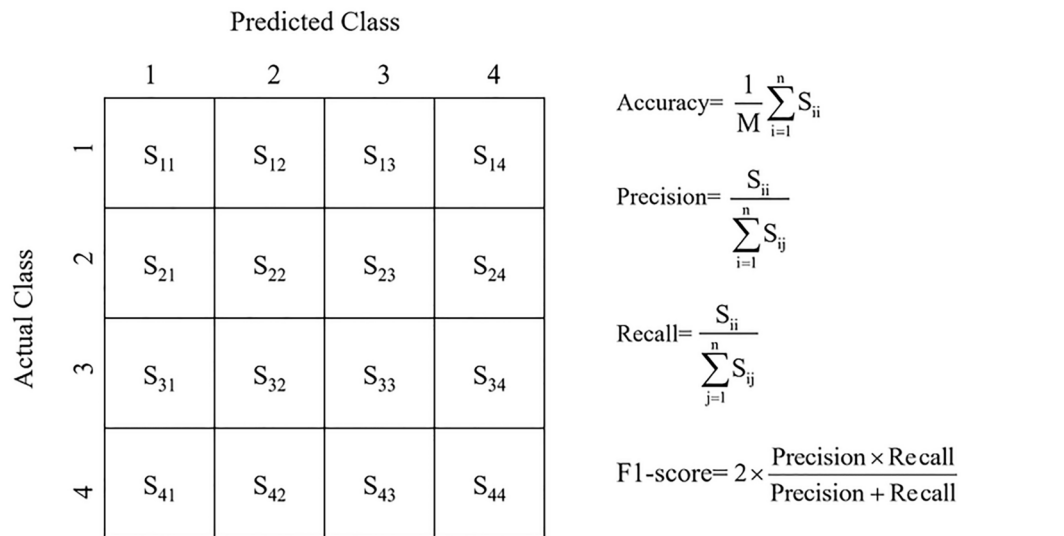


Fig. 3. The RF-WOA/COA hybrid architecture.

Hyperparameter	Description	Min_range	Max_range	Optimum value
<code>n_estimators</code>	number of trees in the forest	6	200	100
<code>max_depth</code>	max number of levels in each decision tree	1	100	22
<code>min_samples_split</code>	min number of data points placed in a node before the node is split	2	20	2
<code>min_samples_leaf</code>	min number of data points allowed in a leaf node	1	20	1
<code>max_features</code>	max number of features considered for splitting a node	0.100	1	0.100
<code>max_leaf_nodes</code>	maximum number of leaf nodes	2	20	10

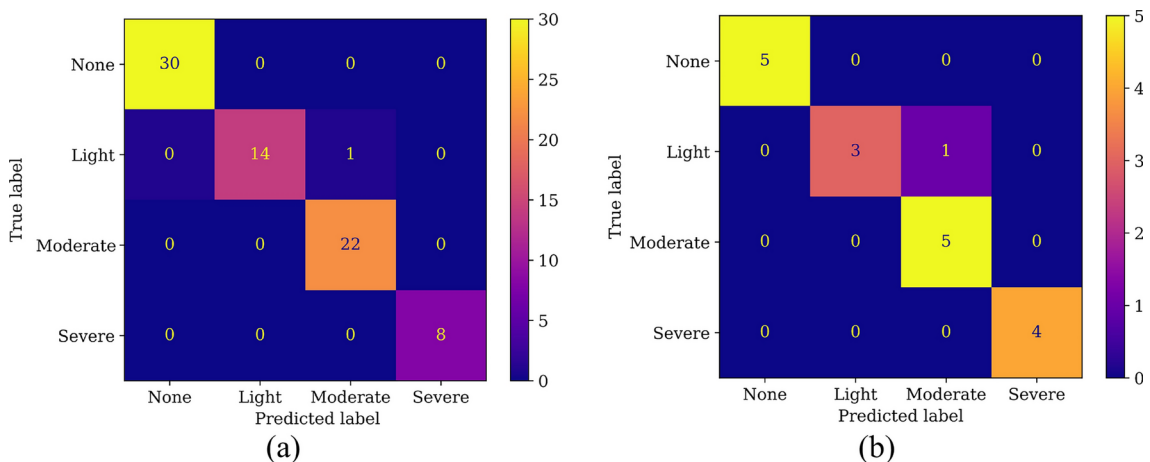
Table 2. The optimal arrangement of RF-WOA hyperparameters.

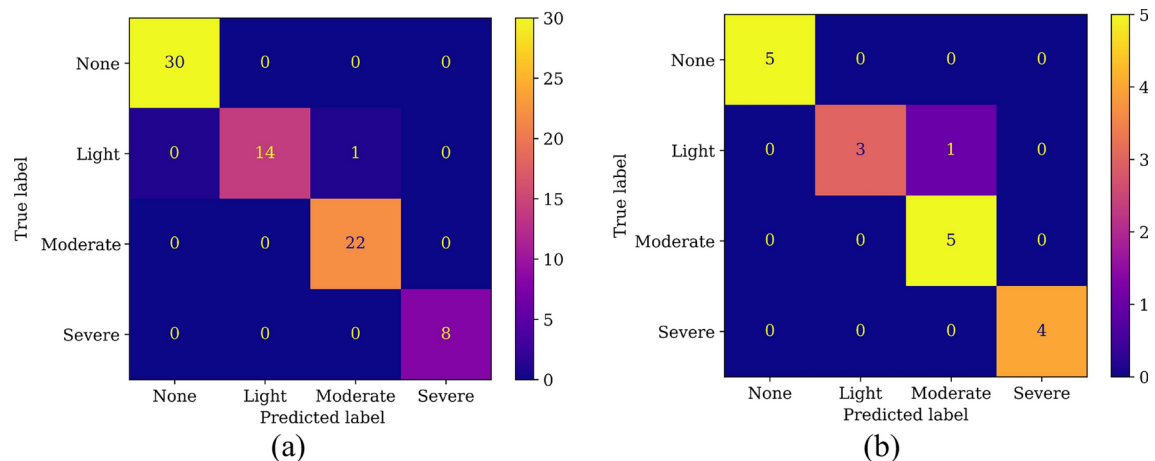
Hyperparameter	Description	Min_range	Max_range	Optimum value
n_estimators	number of trees in the forest	6	200	53
max_depth	max number of levels in each decision tree	1	100	44
min_samples_split	min number of data points placed in a node before the node is split	2	20	8
min_samples_leaf	min number of data points allowed in a leaf node	1	20	4
max_features	max number of features considered for splitting a node	0.100	1	0.600
max_leaf_nodes	maximum number of leaf nodes	2	10	9

Table 3. The optimal arrangement of RF-COA hyperparameters.

n: number of levels

M: number of samples

S_{ii}: number of samples of level i that are correctly predictedS_{ij}: number of samples of level i that are predicted to level j**Fig. 4.** Performance evaluation measures for classification problems^{4,6}.**Fig. 5.** Confusion matrix of RF-WOA model: (a) Training, (b) Testing.

**Fig. 6.** Confusion matrix of RF-COA model: **(a)** Training, **(b)** Testing..

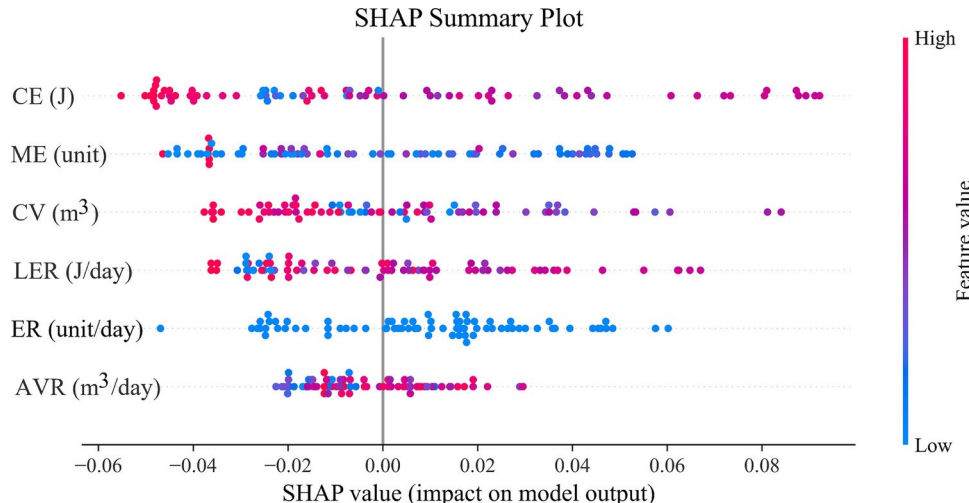
Model	Performance index			
	Accuracy	Precision	Recall	F1-score
RF-WOA	0.944	0.950	0.944	0.943
RF-COA	0.833	0.851	0.788	0.786

Table 4. The performance indices for the developed models.

Researcher	ML method	Hyperparameter tuning	Number of data	Accuracy (%)	Year
Zhou et al. ⁴⁴	Stochastic gradient boosting	tenfold cross validation	254	61.22	2016
Liang et al. ⁶	Random forest, adaptive boosting, gradient boosted decision tree, extreme gradient boosting, and light gradient boosting machine	fivefold cross validation	93	80.0	2020
Li et al. ⁴⁷	Artificial neural network	-	254	71.0	2020
Ji et al. ⁴⁶	Support vector machine	Genetic optimization	132	88.0	2020
Liang et al. ⁶⁶	Logistic regression, naive Bayes, Gaussian process, multilayer perceptron neural network, support vector machines, and decision tree	fivefold cross validation	91	86.6	2021
Yin et al. ⁶⁷	Convolutional neural network	Adaptive moment optimization and Bayes optimization	400	91.67	2021
Maxutov and Adoko ⁶⁸	Bayesian network	-	254	78.0	2021
Kamran et al. ⁶⁹	K-Nearest neighbor	-	93	96.0	2022
Ullah et al. ⁴	Extreme gradient boosting	Grid search	93	88.0	2022
Jin et al. ¹³	Categorical gradient boosting	Grid search	99	89.5	2023
Qiu and Zhou ⁷⁰	Light gradient boosting machine, extreme gradient boosting, random forest, support vector machine, and logistic regression	LévyFlight-Jaya optimization	91	89.3	2023
Qiu and Zhou ⁴⁸	Extreme gradient boosting	Sand cat swarm optimization	254	88.4	2023
Sun et al. ⁷¹	Random forest	-	105	85.7	2023
Sun et al. ⁷²	Weighted probability stacking	Bayesian optimization	114	91.3	2024
This study	Random forest	Coati optimization	93	83.3	2025
This study	Random forest	Whale optimization	93	94.4	2025

Table 5. The comparison between the models generated in this study and the models developed in previous studies.

No	ME (unit)	CE (J)	CV (m ³)	ER (unit/day)	LER (J/day)	AVR (m ³ /day)	RB severity	
							Actual	Predicted
1	23	6.419	4.995	5.750	5.817	4.390	Severe	Severe
2	10	4.886	4.105	1.660	4.107	3.326	Moderate	Moderate
3	11	3.712	4.635	2.200	3.013	3.936	Moderate	Light
4	18	3.828	4.703	3.000	3.046	3.924	Moderate	Light
5	21	5.848	4.834	1.900	4.806	3.792	Moderate	Moderate
6	2	1.940	3.250	2.000	1.920	3.250	None	None
7	13	5.348	4.780	0.920	4.201	3.633	None	None
8	15	3.486	5.030	2.140	2.640	4.180	None	None
9	2	4.061	3.576	0.660	3.583	3.098	Light	None
10	5	5.170	4.594	0.833	4.391	3.815	Light	Light
11	17	3.172	5.015	1.700	2.172	4.015	Light	Light
12	25	4.381	4.848	2.500	3.381	3.848	Light	Light
13	25	3.367	4.964	3.125	2.463	4.060	Light	Light
14	25	4.730	4.310	1.923	3.616	3.196	Light	Light
15	60	5.860	4.730	4.286	4.714	3.584	Moderate	Moderate

Table 6. Validation results of RF-WOA model for 19 new RB cases.**Fig. 7.** The SHAP plot of RF-WOA model.

severity expect for cases 3 and 4, which yields the accuracy of 86.667%. This proves the good generalization and effectiveness of the proposed RF-WOA model.

Model interpretability and parameters importance

Despite the high performance of the developed model, it cannot interpret the effects of local samples on the model output or quantify the correlations between different features, resulting in insufficient explanations for the prediction process. Furthermore, due to its complexity, the model lacks interpretability⁷⁴. Therefore, an integrated model interpretation framework called SHAP is introduced to enhance the understanding of the RB risk prediction mechanism. The framework integrates the Shapley values derived from cooperative game theory with the locally explainable model explanation method. The SHAP method is a recently discovered technique that uses Shapley values to provide explanations for predictions generated by machine learning algorithms⁷⁴. Using the SHAP method, it is possible to determine the specific contributions of the input parameters to the predictive outputs in the model, as well as whether their effects on the results are positive or negative. Although SHAP is generally used for providing local explanations, it is also feasible to get an overall view by analyzing the Shapley values, as shown in Fig. 7. The horizontal axis of Fig. 7 represents the SHAP values, whereas the vertical axis denotes the properties that are pivotal for the prediction made by the model. The color bar represents the feature's precise value. The attributes representing the features along the y-axis are presented in a descending order, where the attribute with the highest mean absolute SHAP value is positioned initially.

Based on the importance of input parameters, ME, CE, and CV have been identified as the most effective parameters in the occurrence of the RB phenomenon. These parameters are fundamental indicators representing

the attributes of microfractures during the development of RB events, as stated in Feng et al.¹⁰. According to the SHAP values of these three parameters (Fig. 7), their dependency plots can be presented to interpret the behavior of this phenomenon. Figure 8 presents the SHAP force plot and waterfall plot. This figure visually demonstrates how the RF-WOA model is gradually adjusted from the base value to the final predicted value through various parameters. In Fig. 8b, the value of $E[f(x)]$ represents the model's baseline (the average predicted output without considering specific parameters), while $f(x)$ indicates the final predicted value for this sample^{75–77}. It can be observed that the CE parameter has a value of +0.09, making it the largest positive contributor to the prediction. As shown in Figs. 8a and 8b, the predicted value matches the actual value, highlighting the high accuracy of the developed model. By quantifying the contribution of features using SHAP values and providing local explanations for individual samples, one can thoroughly investigate the feature-specific effects on a given predictor value, thereby significantly enhancing the model's interpretability. Figure 9 shows the three-dimensional dependency plot of these three parameters. Based on this figure, the behavior of RB (relative to the most effective parameters in the occurrence of this phenomenon) follows a parabolic pattern. According to this figure, when the values of these parameters are low, the risk of RB is also low. Clearly, as the microfracture density, extent of damage, and fracture strength of the rock mass decrease, the burst power of the rock mass decreases as well. Gradually, with the increase in the values of these parameters, the risk of this phenomenon occurring increases. However, when these values surpass a certain limit, the strength of the rock mass increases to a point where the risk of this phenomenon occurring decreases. By identifying this limit, appropriate control measures can be implemented to reduce the potential risk of this phenomenon. This may entail reinforcing the rock mass, implementing ground support systems, or adjusting mining techniques to minimize the likelihood of RB^{53,78}. Understanding the relationship between these parameters and the risk of RB is crucial for ensuring the safety of workers in underground mining operations.

Summary and conclusions

Microseismic activity, mining disturbances, and geological factors influence the occurrence and consequences of RB. Hence, it is crucial to take these influential factors into account when issuing early risk warnings. Furthermore, it is essential to create precise and easily understandable prediction models to improve the dependability and practicality of ML in predicting RB threats. In this study, real-time models for predicting short-term RB have been developed using the powerful RF algorithm and two meta-heuristic algorithms (WOA and COA) to optimally set hyperparameters. To develop the models and implement the algorithm, a database comprising 93 RB case histories was used, taking into account the MS parameters affecting the occurrence of this phenomenon. Finally, to interpret the model, the SHAP method was employed. The performance results of the developed models showed that the RF-WOA model outperformed the RF-COA model (Accuracy=0.944,

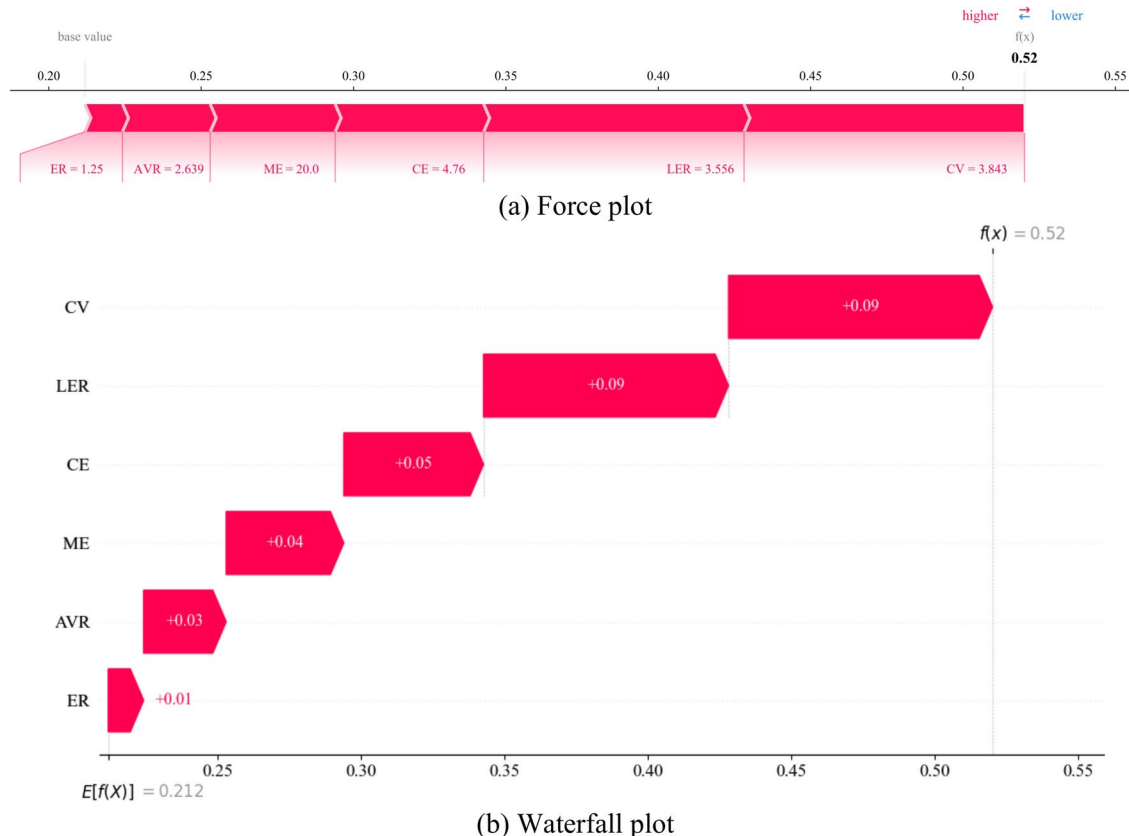


Fig. 8. The SHAP force and waterfall plot.

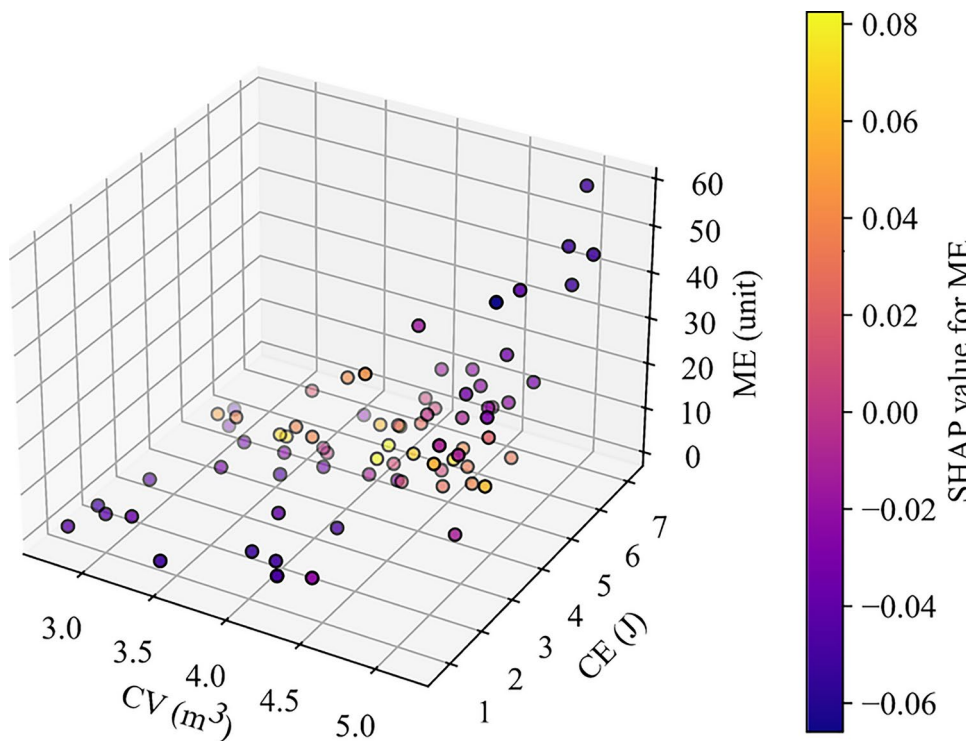


Fig. 9. 3D dependency plot obtained from SHAP analysis for the most effective RB parameters.

Precision = 0.950, Recall = 0.944, and F1-score = 0.943). Additionally, comparing the performance of the RF-WOA model with other previously developed models demonstrated that this model evaluates this phenomenon with high accuracy and low uncertainty. The results of examining the importance of input parameters on the occurrence of this phenomenon showed that three parameters including ME, CE, and CV have the greatest impact on the occurrence of this phenomenon. Finally, by analyzing the SHAP values of these three parameters, it was found that the behavior of this phenomenon follows a parabolic-like pattern. Specifically, at low values of these three parameters, the risk of RB is low. As the values of these parameters increase, the risk of occurrence also increases and finally, after surpassing a certain limit, the risk of occurrence begins to decrease. The obtained results can be a valuable resource for accurately predicting the occurrence of short-term RB in operational conditions. Project managers can implement the necessary control and management measures based on these results to reduce the risk of this phenomenon. However, this study has limitations, such as the number of cases in the database and the lack of examination of geological and mining parameters. The authors are currently studying these parameters, and their inclusion will ensure the comprehensiveness of the models, as investigating this phenomenon thoroughly is essential.

Data availability

The datasets generated during and analyzed during the current study are available from the corresponding author on reasonable request.

Received: 25 May 2024; Accepted: 30 December 2024

Published online: 06 January 2025

References

1. Dietz, M., Oremek, G., Groneberg, D. & Bendels, M. What is a rock burst?. *Zentralblatt für Arbeitsmedizin, Arbeitsschutz und Ergon.* **68**, 45–49 (2018).
2. Cai, M. Principles of rock support in burst-prone ground. *Tunn. Undergr. Sp. Technol.* **36**, 46–56 (2013).
3. Ortlepp, W. D. & Stacey, T. R. Rockburst mechanisms in tunnels and shafts. *Tunn. Undergr. Sp. Technol.* **9**, 59–65 (1994).
4. Ullah, B., Kamran, M. & Rui, Y. Predictive modeling of short-term rockburst for the stability of subsurface structures using machine learning approaches: t-SNE, K-Means Clust, XGBoost. *Math.* **10**, 449 (2022).
5. Liang, W., Zhao, G., Wang, X., Zhao, J. & Ma, C. Assessing the rockburst risk for deep shafts via distance-based multi-criteria decision making approaches with hesitant fuzzy information. *Eng. Geol.* **260**, 105211 (2019).
6. Liang, W., Sari, A., Zhao, G., McKinnon, S. D. & Wu, H. Short-term rockburst risk prediction using ensemble learning methods. *Nat. Hazards* **104**, 1923–1946 (2020).
7. Zhang, Y. et al. Rockburst prediction using artificial intelligence techniques: A review. *Rock Mech. Bull.* **3**, 100129 (2024).
8. Waqar, M. F., Guo, S. & Qi, S. A comprehensive review of mechanisms, predictive techniques, and control strategies of rockburst. *Appl. Sci.* **13**, 3950 (2023).
9. Zhang, M., Liu, S. & Shimada, H. Regional hazard prediction of rock bursts using microseismic energy attenuation tomography in deep mining. *Nat. Hazards* **93**, 1359–1378 (2018).

10. Feng, G. L., Feng, X. T., Chen, B. R., Xiao, Y. X. & Yu, Y. A microseismic method for dynamic warning of rockburst development processes in tunnels. *Rock Mech. Rock Eng.* **48**, 2061–2076 (2015).
11. Feng, G. L., Feng, X. T., Chen, B. R., Xiao, Y. X. & Zhao, Z. N. Effects of structural planes on the microseismicity associated with rockburst development processes in deep tunnels of the Jinping-II Hydropower Station China. *Tunn. Undergr. Sp. Technol.* **84**, 273–280 (2019).
12. Mao, H. et al. Analysis of rockburst mechanism and warning based on microseismic moment tensors and dynamic Bayesian networks. *J. Rock Mech. Geotech. Eng.* **15**, 2521–2538 (2023).
13. Jin, A., Basnet, P. & Mahtab, S. Evaluation of short-term rockburst risk severity using machine learning methods. *Big Data Cogn. Comput.* **7**, 172 (2023).
14. Feng, X.-T. & Wang, L. Rockburst prediction based on neural networks. *Trans. Nonferrous Met. Soc. China* **4**, 7–14 (1994).
15. Zhou, J., Li, X. & Shi, X. Long-term prediction model of rockburst in underground openings using heuristic algorithms and support vector machines. *Saf. Sci.* **50**, 629–644 (2012).
16. Afraei, S., Shahriar, K. & Madani, S. H. Statistical assessment of rock burst potential and contributions of considered predictor variables in the task. *Tunn. Undergr. Sp. Technol.* **72**, 250–271 (2018).
17. Pu, Y., Apel, D. B., Wang, C. & Wilson, B. Evaluation of burst liability in kimberlite using support vector machine. *Acta Geophys.* **66**, 973–982 (2018).
18. Pu, Y., Apel, D. B. & Lingga, B. Rockburst prediction in kimberlite using decision tree with incomplete data. *J. Sustain. Min.* **17**, 158–165 (2018).
19. Shirani Faradonbeh, R. & Taheri, A. Long-term prediction of rockburst hazard in deep underground openings using three robust data mining techniques. *Eng. Comput.* **35**, 659–675 (2018).
20. Wu, S., Wu, Z. & Zhang, C. Rock burst prediction probability model based on case analysis. *Tunn. Undergr. Sp. Technol.* **93**, 103069 (2019).
21. Pu, Y., Apel, D. B. & Xu, H. Rockburst prediction in kimberlite with unsupervised learning method and support vector classifier. *Tunn. Undergr. Sp. Technol.* **90**, 12–18 (2019).
22. Zheng, Y. et al. Rockburst Prediction model based on entropy weight integrated with grey relational BP neural network. *Adv. Civ. Eng.* **2019**, (2019).
23. Ghasemi, E., Gholizadeh, H. & Adoko, A. C. Evaluation of rockburst occurrence and intensity in underground structures using decision tree approach. *Eng. Comput.* **36**, 213–225 (2020).
24. Zhou, J., Guo, H., Koopalipoor, M., Jahed Armaghani, D. & Tahir, M. M. Investigating the effective parameters on the risk levels of rockburst phenomena by developing a hybrid heuristic algorithm. *Eng. Comput.* **1**, 3 (2020).
25. Xue, Y., Bai, C., Qiu, D., Kong, F. & Li, Z. Predicting rockburst with database using particle swarm optimization and extreme learning machine. *Tunn. Undergr. Sp. Technol.* **98**, 103287 (2020).
26. Dong, L. J., Li, X. B., Peng, K. Prediction of rockburst classification using random forest. *Trans. Nonferrous Met. Soc. China English Ed.* **23**, 472–477 (2013).
27. Kadkhodaei, M. H., Ghasemi, E. & Sari, M. Stochastic assessment of rockburst potential in underground spaces using Monte Carlo simulation. *Environ. Earth Sci.* **81**, 1–15 (2022).
28. Kadkhodaei, M. H. & Ghasemi, E. Development of a semi-quantitative framework to assess rockburst risk using risk matrix and logistic model tree. *Geotech. Geol. Eng.* **40**, 3669–3685 (2022).
29. Zhou, J., Zhang, Y., Li, C., He, H. & Li, X. Rockburst prediction and prevention in underground space excavation. *Undergr. Sp.* **14**, 70–98 (2024).
30. ManSinghBasnet, P., Mahtab, S. & Jin, A. A comprehensive review of intelligent machine learning based predicting methods in long-term and short-term rock burst prediction. *Tunn. Undergr. Sp. Technol.* **142**, 105434 (2023).
31. Chen, X. & Yu, H. Rockburst prediction for deep tunneling near fault based on the PD-BEM method. *Tunn. Undergr. Sp. Technol.* **147**, 105725 (2024).
32. Zhang, Q. et al. A semi-Naïve Bayesian rock burst intensity prediction model based on average one-dependent estimator and incremental learning. *Tunn. Undergr. Sp. Technol.* **146**, 105666 (2024).
33. Adoko, A. C. & Zvarivadza, T. A Bayesian Approach for Predicting Rockburst. *52nd US Rock Mechanics/Geomechanics Symposium* at (2018).
34. Wang, A. F., Yang, X. T. & Gu, X. B. The risk assessment of rockburst intensity in the highway tunnel based on the variable fuzzy sets theory. *Sci. Reports* **13**, 1–12 (2023).
35. Sun, L. et al. Ensemble stacking rockburst prediction model based on Yeo-Johnson, K-means SMOTE, and optimal rockburst feature dimension determination. *Sci. Rep.* **12**, 1–16 (2022).
36. Shen, Y., Wu, S., Wang, Y., Wang, J. & Yang, Z. Interpretable model for rockburst intensity prediction based on Shapley values-based Optuna-random forest. *Undergr. Sp.* <https://doi.org/10.1016/J.JUNDSP.2024.09.002> (2024).
37. Gao, W. Forecasting of rockbursts in deep underground engineering based on abstraction ant colony clustering algorithm. *Nat. Hazards* **76**, 1625–1649 (2015).
38. Zhou, J., Li, X. & Mitrí, H. S. Classification of rockburst in underground projects: Comparison of ten supervised learning methods. *J. Comput. Civ. Eng.* **30**, 04016003 (2016).
39. Jiang, K., Lu, J. & Xia, K. A novel algorithm for imbalance data classification based on genetic algorithm improved SMOTE. *Arab. J. Sci. Eng.* **41**, 3255–3266 (2016).
40. Li, N., Feng, X. & Jimenez, R. Predicting rock burst hazard with incomplete data using Bayesian networks. *Tunn. Undergr. Sp. Technol.* **61**, 61–70 (2017).
41. Li, T., Zheng, L. Y., Xin & Yang, X. li. Rock burst prediction based on genetic algorithms and extreme learning machine. *J. Cent. South Univ.* **24**, 2105–2113 (2017).
42. Lin, Y., Zhou, K. & Li, J. Application of cloud model in rock burst prediction and performance comparison with three machine learning algorithms. *IEEE Access* **6**, 30958–30968 (2018).
43. Li, N. & Jimenez, R. A logistic regression classifier for long-term probabilistic prediction of rock burst hazard. *Nat. Hazards* **90**, 197–215 (2018).
44. Zhou, J., Shi, X., Huang, R., Qiu, X., Chen, C. Feasibility of stochastic gradient boosting approach for predicting rockburst damage in burst-prone mines. *Trans. Nonferrous Met. Soc. China English Ed.* **26**, 1938–1945 (2016).
45. Feng, G., Xia, G., Chen, B., Xiao, Y. & Zhou, R. A method for rockburst prediction in the deep tunnels of hydropower stations based on the monitored microseismicity and an optimized probabilistic neural network model. *Sustain.* **11**, 3212 (2019).
46. Ji, B., Xie, F., Wang, X., He, S. & Song, D. Investigate contribution of multi-microseismic data to rockburst risk prediction using support vector machine with genetic algorithm. *IEEE Access* **8**, 58817–58828 (2020).
47. Li, N., Zare Naghadehi, M., Jimenez, R. Evaluating short-term rock burst damage in underground mines using a systems approach. *Int. J. Mining, Reclam. Environ.* **34**, 531–561 (2020).
48. Qiu, Y. & Zhou, J. Short-term rockburst damage assessment in burst-prone mines: An explainable XGBOOST hybrid model with SCSO algorithm. *Rock Mech. Rock Eng.* **56**, 8745–8770 (2023).
49. Vincent, A. M. & Jidesh, P. An improved hyperparameter optimization framework for AutoML systems using evolutionary algorithms. *Sci. Rep.* **13**, 1–19 (2023).
50. Ali, Y. A., Awwad, E. M., Al-Razgan, M. & Maarouf, A. Hyperparameter search for machine learning algorithms for optimizing the computational complexity. *Process.* **11**, 349 (2023).

51. Feng, X., Chen, B., Zhang, C., Li, S. & Wu, S. *Mechanism* (Warning and Dynamic Control of Rockburst Development Processes. Sci. Press Beijing, 2013).
52. Chen, B. R., Feng, X. T., Li, Q. P., Luo, R. Z. & Li, S. Rock burst intensity classification based on the radiated energy with damage intensity at Jinping II hydropower station. *China. Rock Mech. Rock Eng.* **48**, 289–303 (2015).
53. Feng, X.-T., Yashun, X. & Guangliang, F. Mechanism, warning and dynamic control of rockburst evolution process. in *ISRM Regional Symposium - 7th Asian Rock Mechanics Symposium, Seoul, Korea* (OnePetro, 2012).
54. Ma, T. H., Tang, C. A., Tang, L. X., Zhang, W. D. & Wang, L. Rockburst characteristics and microseismic monitoring of deep-buried tunnels for Jinping II Hydropower Station. *Tunn. Undergr. Sp. Technol.* **49**, 345–368 (2015).
55. Breiman, L. Random forests. *Mach. Learn.* **45**, 5–32 (2001).
56. Breiman, L. Bagging predictors. *Mach. Learn.* **24**, 123–140 (1996).
57. Mirjalili, S. & Lewis, A. The whale optimization algorithm. *Adv. Eng. Softw.* **95**, 51–67 (2016).
58. Watkins, W. A. & Schevill, W. E. Aerial observation of feeding behavior in four baleen whales: *Eubalaena glacialis*, *Balaenoptera borealis*, *Megaptera novaeangliae*, and *Balaenoptera physalus*. *J. Mammal.* **60**, 155–163 (1979).
59. He, B., Armaghani, D. J. & Lai, S. H. Assessment of tunnel blasting-induced overbreak: A novel metaheuristic-based random forest approach. *Tunn. Undergr. Sp. Technol.* **133**, 104979 (2023).
60. Zhou, J. et al. Predicting tunnel squeezing using support vector machine optimized by whale optimization algorithm. *Acta Geotech.* **17**, 1343–1366 (2022).
61. Zhao, J., Nguyen, H., Nguyen-Thoi, T., Asteris, P. G. & Zhou, J. Improved Levenberg–Marquardt backpropagation neural network by particle swarm and whale optimization algorithms to predict the deflection of RC beams. *Eng. Comput.* **38**, 3847–3869 (2022).
62. Guo, H., Zhou, J., Koopalipoor, M., Jahed Armaghani, D. & Tahir, M. M. Deep neural network and whale optimization algorithm to assess flyrock induced by blasting. *Eng. Comput.* **37**, 173–186 (2021).
63. Dehghani, M., Montazeri, Z., Trojovská, E. & Trojovský, P. Coati optimization algorithm: A new bio-inspired metaheuristic algorithm for solving optimization problems. *Knowledge-Based Syst.* **259**, 110011 (2023).
64. Wang, K., He, B., Samui, P. & Zhou, J. Predicting rock burst in underground engineering leveraging a novel metaheuristic-based LightGBM model. *Comput. Model. Eng. Sci.* **140**, 229–253 (2024).
65. Han, J., Pei, J. & Kamber, M. *Data Mining: Concepts and Techniques*. (2011).
66. Liang, W., Sari, Y. A., Zhao, G., McKinnon, S. D. & Wu, H. Probability estimates of short-term rockburst risk with ensemble classifiers. *Rock Mech. Rock Eng.* **54**, 1799–1814 (2021).
67. Yin, X., Liu, Q., Huang, X. & Pan, Y. Real-time prediction of rockburst intensity using an integrated CNN-Adam-BO algorithm based on microseismic data and its engineering application. *Tunn. Undergr. Sp. Technol.* **117**, 104133 (2021).
68. Maxutov, K. & Adoko, A. C. Establishing a Bayesian Network model for predicting rockburst damage potential. *IOP Conf. Ser. Earth Environ. Sci.* **861**, 062094 (2021).
69. Kamran, M., Ullah, B., Ahmad, M. & Sabri, M. M. S. Application of KNN-based isometric mapping and fuzzy c-means algorithm to predict short-term rockburst risk in deep underground projects. *Front. Public Heal.* **10**, 1023890 (2022).
70. Qiù, Y. & Zhou, J. Short-term rockburst prediction in underground project: insights from an explainable and interpretable ensemble learning model. *Acta Geotech.* **18**, 6655–6685 (2023).
71. Sun, J., Wang, W. & Xie, L. Predicting short-term rockburst using RF–CRITIC and improved cloud model. *Nat. Resour. Res.* **33**, 471–494 (2024).
72. Sun, J., Wang, W. & Xie, L. Predicting short-term rockburst intensity using a weighted probability stacking model with optimal feature selection and Bayesian hidden layer. *Tunn. Undergr. Sp. Technol.* **153**, 106021 (2024).
73. Jin, A., Basnet, P. M. S. & Mahtab, S. Microseismicity-based short-term rockburst prediction using non-linear support vector machine. *Acta Geophys.* **70**, 1717–1736 (2022).
74. Lundberg, S. & Lee, S.-I. A Unified Approach to Interpreting Model Predictions. *Adv. Neural Inf. Process. Syst.* **4766–4775** (2017).
75. Lubo-Robles, D. et al. Machine learning model interpretability using SHAP values: Application to a seismic facies classification task. *SEG Int. Expo. Annu. Meet. 2020–Octob*, 1460–1464 (2020).
76. Antonini, A. S. et al. Machine learning model interpretability using SHAP values: Application to igneous rock classification task. *Appl. Comput. Geosci.* **23**, 100178 (2024).
77. Zhang, K., Xu, P. & Zhang, J. Explainable AI in deep reinforcement learning models: A SHAP method applied in power system emergency control. *2020 IEEE 4th Conf. Energy Internet Energy Syst. Integr. Connect. Grids Towar. a Low-Carbon High-Efficiency Energy Syst. EI2 2020* 711–716 (2020) <https://doi.org/10.1109/EI250167.2020.9347147>.
78. Li, N., Huang, B., Zhang, X., Yuyang, T. & Li, B. Characteristics of microseismic waveforms induced by hydraulic fracturing in coal seam for coal rock dynamic disasters prevention. *Saf. Sci.* **115**, 188–198 (2019).

Author contributions

Mohammad Hossein Kadkhodaei: Writing-original draft, methodology, Data collection, Data preparation, validation, software, visualization. Ebrahim Ghasemi: Conceptualization, supervision, review and editing, formal analysis, Discussion. All authors reviewed the manuscript.

Funding

The authors declare that no funds, grants, or other support were received during the preparation of this manuscript.

Declarations

Competing interests

The authors declare no competing interests.

Additional information

Correspondence and requests for materials should be addressed to M.H.K.

Reprints and permissions information is available at www.nature.com/reprints.

Publisher's note Springer Nature remains neutral with regard to jurisdictional claims in published maps and institutional affiliations.

Open Access This article is licensed under a Creative Commons Attribution-NonCommercial-NoDerivatives 4.0 International License, which permits any non-commercial use, sharing, distribution and reproduction in any medium or format, as long as you give appropriate credit to the original author(s) and the source, provide a link to the Creative Commons licence, and indicate if you modified the licensed material. You do not have permission under this licence to share adapted material derived from this article or parts of it. The images or other third party material in this article are included in the article's Creative Commons licence, unless indicated otherwise in a credit line to the material. If material is not included in the article's Creative Commons licence and your intended use is not permitted by statutory regulation or exceeds the permitted use, you will need to obtain permission directly from the copyright holder. To view a copy of this licence, visit <http://creativecommons.org/licenses/by-nc-nd/4.0/>.

© The Author(s) 2025